Available online at www.sciencedirect.com
ScienceDirect
Journal of Sound and Vibration 321 (2009) 1036–1057
JOURNAL OF SOUND AND VIBRATION
www.elsevier.com/locate/jsvi

Dual reciprocity hybrid boundary node method for free vibration analysis

F. Yan[a], Y.H. Wang[a,*], Y. Miao[a], Y.K. Cheung[b]

[a]*School of Civil Engineering and Mechanics, Huazhong University of Science and Technology, Wuhan, Hubei 430074, PR China*
[b]*Department of Civil Engineering, University of Hong Kong, Hong Kong, PR China*

Received 14 September 2007; received in revised form 11 October 2008; accepted 17 October 2008
Handling Editor: J. Lam
Available online 29 November 2008

Abstract

As a truly meshless method of boundary-type, the hybrid boundary node method (HBNM) has the advantages of both boundary element method (BEM) and meshless method. The main problem is that it is only suitable for the homogeneous problems. Now, the dual reciprocity method (DRM) is introduced into HBNM to deal with the integral for the inhomogeneous terms of the governing equations, and the rigid body motion approach is employed to solve the hyper-singular integrations. A new meshless method named dual reciprocity hybrid boundary node method (DRHBNM) is proposed and applied to solve free vibration problems. In this method, the solution composes into two parts, i.e., the general solution and the particular solution. The general solution is solved by HBNM and the particular one is obtained by DRM. DRHBNM is a true boundary-type meshless method. It does not require the 'boundary element mesh', either for the purpose of interpolation of the variables, or for the integration of 'energy'. The points in the domain are only used to interpolate particular solution by the radial basis function. Finally, the boundary variables are interpolated by the independent smooth boundary segments. The Q–R algorithm and Householder algorithm are applied to solve the eigenvalues and eigenvectors of the transformed matrix.

Numerical examples for free vibration problems show that a good convergence with mesh refinement is achievable and the computational results for the natural circular frequencies and free vibration modes are very accurate. Furthermore, the computation parameters have little influence on the results and can be chosen in a wide range. It is shown that the present method is effective and can be widely applied in practical engineering.

1. Introduction

Oscillation phenomenon is a common problem in mechanical and civil engineering. Most of the structures do not expect the occurrence of vibration, which can cause fatigue failure. In the analysis the natural circular frequency and free vibration modes are the characters that must be learned for structural analysis. In order to avoid sympathetic vibration, the load frequency must be not close to the natural frequency of the structure. As the geometrical and loading conditions are complex, it is difficult to obtain the analytical solutions usually.

*Corresponding author. Tel.: +86 27 87542860; fax: +86 27 87542231.
E-mail address: yhwang0062@163.com (Y.H. Wang).

0022-460X/$ - see front matter © 2008 Elsevier Ltd. All rights reserved.
doi:10.1016/j.jsv.2008.10.018

Therefore, the studies on numerical methods for the free vibration make great significance to the practical engineering applications.

Numerical methods have been developed rapidly in the past decades. Those methods include finite element method (FEM), boundary element method (BEM), finite difference method, meshless method, etc. As a popular tool, FEM [1] has been well developed in the past decades. Also, because of 'boundary only' and high accuracy properties, BEM [2] appears to be an attractive alternative. Compared with FEM and BEM, the meshless method does not require elements and thus attracts more and more attention in the recent years. It has a series of advantages such as flexibility, efficiency, and versatility for complex geometry of solids and different engineering problems, including large deformation and crack propagation.

The meshless method is a great variety and can be divided into two types, i.e., the domain-type and the boundary-type. For the domain-type, there are the diffuse element method (DEM) [3], the element free Galerkin (EFG) method [4], the reproducing kernel particle method (RKPM) [5], the point interpolation method (PIM) [6], the meshless local Petrov–Galerkin (MLPG) method [7], the local point interpolation method (LPIM) [8], the method of finite spheres (MFS) [9] and the finite cloud method (FCM) [10]. On the other hand, the boundary-type includes the local boundary integral equation method (LBIEM) [11], the boundary node method (BNM) [12], the boundary radial basis function method (BRBFM) [13] and the boundary point interpolation method (BPIM) [14].

Though all meshless methods do not need the element mesh for the field variable interpolation, some of them require a background mesh for integration. For example, the EFG method uses MLS for the shape function interpolation, and it does not require element mesh. However, background element is inevitable for integration.

Mukherjee et al. proposed BNM [15] and applied MLS to the boundary integration equations. It only requires to discretized the boundary. Although this method does not require an element mesh for the interpolation of the boundary variables, a background element is still necessary for integration.

Based on BNM, Zhang and Yao [16] proposed another boundary-type meshless method: hybrid boundary node method (HBNM). It gets rid of the background elements and achieves a truly meshless method. It uses MLS to approximate the boundary variables, and the integration is limited to a fixed local region. Elements are required neither interpolation nor integration. Zhang and Yao [17–19] applied it to the potential problems and some homogeneous elasticity problems. However, it has a drawback of serious 'boundary layer effect', i.e., the accuracy of the result near the boundary is very sensitive to the proximity of the interior points nearby the boundary.

To avoid this shortcoming, Zhang and Yao further proposed the regular hybrid boundary node method [20,21]. Compared with HBNM in which the source points are located on the boundary, the source points of the fundamental solution in this method are located outside of the domain. However, it requires a new parameter, namely scale factor S_f, which decides the distance between the source point of the fundamental solution and the boundary. Although this method can avoid the singular integration and boundary layer effect, it creates some new problems. For example, how to decide the scale factor value? The numerical examples show that high or low values may lead to errors in the results. Another problem is how to arrange the positions of the source points. The problems may become more obvious for the concave boundary and crack problems.

To overcome these problems, Wang et al. [18] presented a meshless singular hybrid node method for two-dimensional (2-D) elasticity, and obtained satisfactory results by means of reasonable treatment of nearly singular integrals. And Miao [22] proposed the rigid body motion approach to deal with the singular integration and applied an adaptive integration scheme to solve the boundary layer effect. This method, however, can only be used for solving homogeneous problems. For the inhomogeneous problem and dynamic problem, the domain integration is inevitable.

For free vibration problem, the governing equation has a time dependent inhomogeneous term. HBNM cannot solve them without domain integral, which makes the method lose its 'boundary-only' and true meshless character. An initial restriction of HBNM is that the fundamental solution for the original partial differential equation is required to obtain a local integral equation. On the other hand, as a time-dependent problem, the fundamental solution is difficult to obtain. The inhomogeneous terms accounting distributed loads and time dependent term are included in the formulae of the domain integrals. Thus the method loses the attraction of its 'boundary-only' and truly meshless method character.

DRM was introduced by Nardini and Brebbia [23] for elasto-dynamic problems in 1982 and extended by Wrobel and Brebbia [24] to time dependent diffusion in 1986. The method is essentially a generalized way of constructing particular solution that can be used to solve the nonlinear and time-dependent problems as well as to represent any internal source distribution. The method can be applied to define sources over the whole domain or only on part of it. The aim of DRM is to avoid the domain integral that comes out from the inhomogeneous term of the equations. In the case of elasticity, it is the body force. DRM takes advantage of this fact and builds an approximated particular solution in terms of a linear combination of the radial basis function.

In this paper, a truly meshless method is developed for free vibration problem. The method is formed by the combination of HBNM and DRM, and named as dual reciprocity hybrid boundary node method (DRHBNM). The solution composes two parts: general solution and particular solution. For the first part, same as HBNM, the variables inside the domain are interpolated by the fundamental solution, while the unknown boundary variables are approximated by the MLS approximation. The modified variational formulation is applied to form the discretized equations of HBNM. For the second part, DRM has been used and the radial basis functions are applied to interpolating the inhomogeneous part of the equations. Because of the acceleration term of the governing equations, the boundary integral equations obtained by DRHBNM are not enough to solve all variables. Some additional equations are proposed to obtain the relation of the variables in the domain and on the boundary. They are obtained by interpolation of the fundamental solution and the basis form of the particular solutions. The Q–R algorithm and Householder algorithm [25–27] are applied to solving the eigenvalues and eigenvectors of the transformed matrix. In order to overcome the singular integration, the rigid body moving method has been applied. The basic idea of this approach is to employ a fundamental solution corresponding to a simpler equation and to treat the remaining terms, as well as other nonhomogeneous terms in the original equation. The method keeps the 'boundary-only' and truly meshless method character of HBNM. Numerical examples presented give some solutions of free vibration problems such as the circular frequencies and modes.

Compared to FEM and BEM, which are based on elements, DRHBNM is a truly meshless method, which is no need elements meshing and is suit for the dynamic crack problem. Besides, the accuracy and convergence are very high, the numerical examples show that although much less amount of nodes are used, very good results can be obtained comparing with FEM. For the free vibration problems, only some nodes are needed for the analysis and the meshing work is much less, especial for some complex geometry structures. This means the precondition and post treatment are easier than that of FEM.

This paper is organized as follows: Sections 2 and 3 give the outlines of HBNM and DRM. In Section 4, the DRHBNM for elasto-dynamics is formulated. Numerical implementation is demonstrated in Section 5. Numerical examples for 2-D free vibration problems are shown in Section 6. Finally, the paper will end with conclusions in Section 7.

2. Hybrid boundary node method

2.1. Basic equations of elasto-dynamics

Consider a 2-D vibration problem of linear elasticity in domain Ω bounded by Γ, as shown in Fig. 1. The governing equation is

$$\sigma_{ij,j} + b_i = c\dot{u}_i + \rho\ddot{u}_i \tag{1}$$

where ρ is the density of the material and c is the damping coefficient, σ_{ij} is the stress tensor corresponding to the displacement field u_i, b_i is the body force. $\ddot{u}_i = \partial^2 u_i/\partial t^2$ and $\dot{u}_i = \partial u_i/\partial t$ and $(),_i$ denotes $\partial()/\partial x_i$.

The corresponding boundary and initial conditions can be given as

$$u_i = \bar{\bar{u}}_i \quad \text{on the essential boundary } \Gamma_u \tag{2}$$

$$\sigma_{ij}n_j = \bar{\bar{t}}_i \quad \text{on the natural boundary } \Gamma_t \tag{3}$$

$$u(x, t_0) = u_0(x) \tag{4}$$

$$\dot{u}(x, t_0) = v_0(x) \tag{5}$$

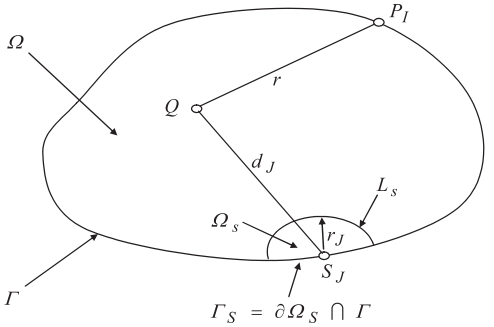

Fig. 1. Local domain and source points corresponding to s_J.

where $\bar{\bar{u}}_i$ and $\bar{\bar{t}}_i$ are the prescribed displacement and traction, u_0 and v_0 are the initial displacement and velocity at the initial time t_0, respectively, n_j is the unit outward normal to the boundary Γ ($\Gamma = \Gamma_u = \Gamma_t$).

For free vibration, c and b_i in Eq. (1) are set equal to zero, the governing equation for the free vibration without damping is rewritten as

$$\sigma_{ij,j} = \rho\ddot{u}_i \tag{6}$$

From the equation above, one can obtain two second-order partial differential equations for the displacement components and can be written in the form

$$Gu_{i,kk} + \frac{G}{1-2v}u_{k,ki} = \rho\ddot{u}_i \tag{7}$$

where $G = E/2(1+v)$ is the shear modulus and v is the Poisson ratio.

Applying DRM, the variables u_i can be divided into two parts, i.e., the general solution u_i^c and particular solution u_i^p, that is

$$u_i = u_i^c + u_i^p \tag{8}$$

The particular solution u_i^p has to satisfy the inhomogeneous equation as

$$Gu_{i,kk}^p + \frac{G}{1-2v}u_{k,ki}^p = \rho\ddot{u}_i \tag{9}$$

On the other hand, the general solution u_i^c must satisfy the homogeneous equation and the modified boundary conditions. It can be written in the form

$$Gu_{i,kk}^c + \frac{G}{1-2v}u_{k,ki}^c = 0 \tag{10}$$

$$u_i^c = \bar{\bar{u}}_i^c = \bar{\bar{u}}_i - u_i^p \tag{11}$$

$$t_i^c = \bar{\bar{t}}_i^c = \bar{\bar{t}}_i - t_i^p \tag{12}$$

2.2. Hybrid boundary node method

HBNM is based on the modified variational principle in which there are three independent filed variables [16,17]:

(1) Displacement in the domain, $\mathbf{u}$, with components u_i
(2) Boundary displacement, $\tilde{\mathbf{u}}$, with component $\tilde{u}_i$.
(3) Boundary tractions, $\tilde{\mathbf{t}}$, with component $\tilde{t}_i$.

As a true boundary-type meshless method, HBNM uses MLS to interpolate the boundary variables and applied fundamental solution interpolation to get variables in the domain.

By using MLS principle, the interpolation function can be written as

$$\tilde{u}(s) = \sum_{i=1}^{n} \Phi_i \hat{u}_i \tag{13}$$

$$\tilde{t}(s) = \sum_{i=1}^{n} \Phi_i \hat{t}_i \tag{14}$$

where

$$\Phi_i(s) = \sum_{j=1}^{m} p_j(s)[A^{-1}(s)B(s)]_{ji} \tag{15}$$

Matrices **A**(**s**) and **B**(**s**) are being defined as

$$\mathbf{A}(\mathbf{s}) = \mathbf{p}^{\mathrm{T}}(\mathbf{s})\mathbf{w}(\mathbf{s})\mathbf{p}(\mathbf{s}) \tag{16}$$

$$\mathbf{B}(\mathbf{s}) = \mathbf{p}^{\mathrm{T}}(\mathbf{s})\mathbf{w}(\mathbf{s}) \tag{17}$$

where **w**(**s**) is the weight matrix for the boundary variables. This is a diagonal matrix and the diagonal elements $w_I(s)$. **p**(**s**) is a vector of the basis function of interpolation. In the following a three-order polynomial basis is used, i.e.,

$$\mathbf{p}^{\mathrm{T}}(\mathbf{s}) = [1, s, s^2, s^3], \quad m = 4 \tag{18}$$

where s is a parameter coordinate and denotes the distance between the point in the domain and the start point on the boundary.

The weight functions play an important role in the meshless methods. Most meshless weight functions are bell-shaped. In the present study, Gaussian weight function is chosen and can be written as

$$w_I(s) = \begin{cases} \dfrac{\exp[-(d_I/c_I)^2] - \exp[-(\hat{d}_I/c_I)^2]}{1 - \exp[-(\hat{d}_I/c_I)^2]}, & 0 \leqslant d_I \leqslant \hat{d}_I \\ 0, & d_I \geqslant \hat{d}_I \end{cases} \tag{19}$$

where $d_I = |s - s_I|$ is the distance between an evaluation point and node s_I, c_I is a constant controlling the shape of the weight function $w_I(s)$ and, therefore, is the relative weights, and $\hat{d}_I$ is the size of the support for the weight function $w_I(s)$ and determines the support of node s_I.

MLS approximation is well defined only when matrix **A** in Eq. (15) is nonsingular. So the boundary variables can be represented as

$$\tilde{\mathbf{u}} = \begin{Bmatrix} \tilde{u}_1 \\ \tilde{u}_2 \end{Bmatrix} = \sum_{I=1}^{N} \begin{bmatrix} \Phi_I(s) & 0 \\ 0 & \Phi_I(s) \end{bmatrix} \begin{Bmatrix} \hat{u}_1^I \\ \hat{u}_2^I \end{Bmatrix} \tag{20}$$

$$\tilde{\mathbf{t}} = \begin{Bmatrix} \tilde{t}_1 \\ \tilde{t}_2 \end{Bmatrix} = \sum_{I=1}^{N} \begin{bmatrix} \Phi_I(s) & 0 \\ 0 & \Phi_I(s) \end{bmatrix} \begin{Bmatrix} \hat{t}_1^I \\ \hat{t}_2^I \end{Bmatrix} \tag{21}$$

where N is the number of nodes of each smooth segment boundary, $\Phi_I(s)$ is the shape function and $\hat{u}_1^I$, $\hat{u}_2^I$, $\hat{t}_1^I$, $\hat{t}_2^I$ are the boundary nodes values.

The domain variables **u** and **t** are interpolated by the fundamental solution, and can be written as

$$\mathbf{u} = \begin{Bmatrix} u_1 \\ u_2 \end{Bmatrix} = \sum_{I=1}^{N_t} \begin{bmatrix} u_{11}^I & u_{12}^I \\ u_{21}^I & u_{22}^I \end{bmatrix} \begin{Bmatrix} x_1^I \\ x_2^I \end{Bmatrix} \tag{22}$$

$$\mathbf{t} = \begin{Bmatrix} t_1 \\ t_2 \end{Bmatrix} = \sum_{I=1}^{N_t} \begin{bmatrix} t_{11}^I & t_{12}^I \\ t_{21}^I & t_{22}^I \end{bmatrix} \begin{Bmatrix} x_1^I \\ x_2^I \end{Bmatrix} \tag{23}$$

where x_i^I is the unknown parameter, N_t is the total boundary number, u_{ij}^I and t_{ij}^I are the fundamental solutions with the source point of P_I (Fig. 1).

The fundamental solution of the 2-D plane strain elasticity problem is given by Refs. [17,18]

$$u_{ij}^I = \frac{-1}{8\pi(1-v)G}[(3-4v)\delta_{ij}\ln(r) - r_{,i}r_{,j}] \tag{24}$$

$$t_{ij}^I = \frac{-1}{4\pi(1-v)r}\left\{[(1-2v)\delta_{ij} + 2r_{,i}r_{,j}]\frac{\partial r}{\partial n} + (1-2v)(r_{,i}n_j - r_{,j}n_i)\right\} \tag{25}$$

where δ is the Kronecker delta function, r is the distance between the source point and the field point and n is the normal to the boundary.

Assuming $b_i = \rho\ddot{u}_i$ in Eq. (9) and applying the principle of the minimum potential energy, the total potential energy Π can be given as [16,17]

$$\Pi = \int_\Omega \frac{1}{2}u_{i,j}c_{ijkl}u_{k,l}\,\mathrm{d}\Omega - \int_\Omega \mathbf{u}^{\mathrm{T}}\mathbf{b}\,\mathrm{d}\Omega - \int_{\Gamma_t}\mathbf{u}^{\mathrm{T}}\bar{\bar{\mathbf{t}}}\,\mathrm{d}\Gamma \tag{26}$$

where $\mathbf{u}$ is the displacement vector, and c_{ijkl} can be written as

$$c_{ijkl} = \frac{2Gv}{1-2v}\delta_{ij}\delta_{kl} + G\delta_{il}\delta_{jk} \tag{27}$$

Eq. (26) should also satisfy the boundary compatibility condition

$$\tilde{\mathbf{u}} = \mathbf{u} \quad \text{on } \Gamma_u \tag{28}$$

where $\tilde{\mathbf{u}}$ is the displacement on the boundary, and $\mathbf{u}$ is the displacement in the domain but very close to the boundary.

For the general solution, Eq. (10) is satisfied where the inhomogeneous term $b_i = 0$. The compatibility condition (28), is introduced into the variational expression (26) by a set of the Lagrange multipliers λ. It can be concluded that the Lagrange multipliers λ represent the tractions on the boundary. Thus, the modified variational principle without body force can be written as

$$\Pi = \int_\Omega \frac{1}{2}u_{i,j}c_{ijkl}u_{k,l}\,\mathrm{d}\Omega - \int_\Omega \tilde{t}_i(u_i - \tilde{u}_i)\,\mathrm{d}\Omega - \int_{\Gamma_t}\tilde{u}_i\bar{\bar{t}}_i\,\mathrm{d}\Gamma \tag{29}$$

Taking the variational of Eq. (29), we have

$$\delta\Pi = \int_\Omega -\sigma_{ij,j}\delta u_i\,\mathrm{d}\Omega + \int_\Gamma (t_i - \tilde{t}_i)\delta u_i\,\mathrm{d}\Gamma - \int_\Gamma (u_i - \tilde{u}_i)\delta\tilde{t}_i\,\mathrm{d}\Gamma - \int_{\Gamma_t}(\tilde{t}_i - \bar{\bar{t}}_i)\delta\tilde{u}_i\,\mathrm{d}\Gamma \tag{30}$$

Let $\delta\Pi = 0$, the following integration equations can be obtained as

$$\int_\Gamma (t_i - \tilde{t}_i)\delta u_i\,\mathrm{d}\Gamma - \int_\Omega \sigma_{ij,j}\delta u_i\,\mathrm{d}\Omega = 0 \tag{31}$$

$$\int_\Gamma (u_i - \tilde{u}_i)\delta\tilde{t}_i\,\mathrm{d}\Gamma = 0 \tag{32}$$

$$\int_{\Gamma_t}(\tilde{t}_i - \bar{\bar{t}}_i)\delta\tilde{u}_i\,\mathrm{d}\Gamma = 0 \tag{33}$$

If the traction boundary condition, $\tilde{t}_i = \bar{\bar{t}}_i$, is imposed, Eq. (33) will be satisfied and it would be ignored in the following analysis.

Because the variational principle is a universal theory, Eqs. (31) and (32) should be satisfied in any sub-domain Ω_s, which is bounded by Γ_s and L_s (Fig. 1). Following Refs. [4,12], the weak forms on a sub-domain Ω_s and its boundary Γ_s and L_s are used to replace Eqs. (31) and (32). At the same time, test function $h_J(Q)$ is used

to replace the variational part. They can be presented as

$$\int_{\Gamma_S+L_S}(t_i-\tilde{t}_i)h_J(Q)\,\mathrm{d}\Gamma-\int_{\Omega_S}\sigma_{ij,j}h_J(Q)\,\mathrm{d}\Omega=0 \tag{34}$$

$$\int_{\Gamma_S+L_S}(u_i-\tilde{u}_i)h_J(Q)\,\mathrm{d}\Gamma=0 \tag{35}$$

The shape and dimension of the sub-domains may be arbitrary. Obviously, a circle is the simplest regularly shaped sub-domain in the 2-D space. The sub-domain Ω_s is chosen as the intersection of domain Ω and a circle centered at a boundary node s_J, and the radius of the circle is r_J (Fig. 1).

In Eqs. (34) and (35), the variables of $\tilde{u}_i$ and $\tilde{t}_i$ on L_s are not defined. If $h_J(Q)$ can be selected in such a way that the integral over L_s vanishes, the problem can be solved successfully. Thus, test function $h_J(Q)$ can be written in the form

$$h_J(Q)=\begin{cases}\dfrac{\exp[-(d_J/c_J)^2]-\exp[-(r_J/c_J)^2]}{1-\exp[-(r_J/c_J)^2]}, & 0\leqslant d_J\leqslant r_J\\ 0, & d_J\geqslant r_J\end{cases} \tag{36}$$

where d_J is the distance between the integral point Q in the domain and the nodal point s_J and c_J is a constant controlling the test function shape. On L_s, $d_J=r_J$; from Eq. (36) it can be seen that $h_J(Q)$ vanishes on boundary L_s.

Eqs. (34) and (35) can be written as

$$\int_{\Gamma_S}(t_i-\tilde{t}_i)h_J(Q)\,\mathrm{d}\Gamma-\int_{\Omega_S}\sigma_{ij,j}h_J(Q)\,\mathrm{d}\Omega=0 \tag{37}$$

$$\int_{\Gamma_S}(u_i-\tilde{u}_i)h_J(Q)\,\mathrm{d}\Gamma=0 \tag{38}$$

It is obvious that the second term of Eq. (37) only has distribution to the principal diagonal of the matrix. From Eqs. (20)–(23), Eqs. (37) and (38) can be rewritten as

$$\sum_{I=1}^{N_t}\int_{\Gamma_S}\begin{bmatrix}t_{11}^I & t_{12}^I\\ t_{21}^I & t_{22}^I\end{bmatrix}\begin{Bmatrix}x_1^I\\ x_2^I\end{Bmatrix}h_J(Q)\,\mathrm{d}\Gamma=\sum_{I=1}^{N_t}\int_{\Gamma_S}\begin{bmatrix}\Phi_I(s) & 0\\ 0 & \Phi_I(s)\end{bmatrix}\begin{Bmatrix}\hat{t}_1^I\\ \hat{t}_2^I\end{Bmatrix}h_J(Q)\,\mathrm{d}\Gamma \tag{39}$$

$$\sum_{I=1}^{N_t}\int_{\Gamma_S}\begin{bmatrix}u_{11}^I & u_{12}^I\\ u_{21}^I & u_{22}^I\end{bmatrix}\begin{Bmatrix}x_1^I\\ x_2^I\end{Bmatrix}h_J(Q)\,\mathrm{d}\Gamma=\sum_{I=1}^{N_t}\int_{\Gamma_S}\begin{bmatrix}\Phi_I(s) & 0\\ 0 & \Phi_I(s)\end{bmatrix}\begin{Bmatrix}\hat{u}_1^I\\ \hat{u}_2^I\end{Bmatrix}h_J(Q)\,\mathrm{d}\Gamma \tag{40}$$

Using the above equations for all nodes, the system equations can be written in the form

$$\mathbf{Tx}=\mathbf{H}\hat{\mathbf{t}}^{\mathbf{c}} \tag{41}$$

$$\mathbf{Ux}=\mathbf{H}\hat{\mathbf{u}}^{\mathbf{c}} \tag{42}$$

where

$$\mathbf{T_{JI}}=\int_{\Gamma_S^J}\begin{bmatrix}t_{11}^I & t_{12}^I\\ t_{21}^I & t_{22}^I\end{bmatrix}h_J(Q)\,\mathrm{d}\Gamma \tag{43}$$

$$\mathbf{H_{JI}}=\int_{\Gamma_S^J}\begin{bmatrix}\Phi_I(s) & 0\\ 0 & \Phi_I(s)\end{bmatrix}h_J(Q)\,\mathrm{d}\Gamma \tag{44}$$

$$\mathbf{U_{JI}}=\int_{\Gamma_S^J}\begin{bmatrix}u_{11}^I & u_{12}^I\\ u_{21}^I & u_{22}^I\end{bmatrix}h_J(Q)\,\mathrm{d}\Gamma \tag{45}$$

Matrices **U** and **T** in the present method are much simpler than those obtained in BEM and BNM. Because the variables interpolation is on the independent boundary segment, matrix **H** is also sparse.

3. Dual reciprocity method

DRM can be used in dynamic problem to transform the domain integral arising from the application of the time-dependent term into the equivalent boundary integrals. In this section, it will be developed to solve the particular solution and introduced into HBNM.

According to the interpolation for the inhomogeneous term, the acceleration approximation should be interpolated both on the boundary and in the domain. Therefore, the approximation of the term $\rho\ddot{u}_k$ can then be proposed as [19,20]

$$\rho\ddot{u}_k \approx \sum_{j=1}^{N+L} f^j \alpha_k^j \quad (k=1,2) \tag{46}$$

where $\alpha_k{}^j$ are a set of initially unknown coefficients, f^j are the approximation functions, N and L are the total numbers of the boundary nodes and the interior nodes, respectively.

The particular solution can be interpolated by the basis form of the particular solution as [19,20]

$$u_k^p \approx \sum_{j=1}^{N+L} \alpha_l^j \overline{u}_{lk}^j \tag{47}$$

If the particular solution $\overline{u}_{km}^j$ satisfies Eq. (9), the following equation can be obtained

$$G\overline{u}_{mk,ll}^j + \frac{G}{1-2v}\overline{u}_{lk,lm}^j = \delta_{mk} f^j \tag{48}$$

Eq. (46) can be rewritten as

$$\boldsymbol{\alpha} = \rho \mathbf{F}^{-1}\ddot{\mathbf{u}} \tag{49}$$

where each column of **F** consists of a vector f^j, which contains the values of f^j at each DRM collocation point.

The approximating function, f, can be chosen as

$$f^j = 1 + r \tag{50}$$

The function f was adopted first by Nardini and Brebbia and then by most researchers as the simplest and most accurate alternative [19–22]. In the present study it is used to solve the basis form of the particular solution.

The particular solution $\overline{u}$ satisfying Eq. (48) is given by Refs. [19–22]

$$\overline{u}_{km} = \frac{1-2v}{(5-4v)G} r_{,m} r_{,k} r^2 + \frac{1}{30(1-v)G}\left[\left(3 - \frac{10v}{3}\right)\delta_{mk} - r_{,m} r_{,k}\right] r^3 \tag{51}$$

The corresponding expression for traction $\overline{t}$ is

$$\begin{aligned}\overline{t}_{km} = {} & \frac{2(1-2v)}{(5-4v)}\left[\frac{1+v}{1-2v} r_{,m} n_k + \frac{1}{2} r_{,k} n_m + \frac{1}{2}\delta_{mk}\frac{\partial r}{\partial n}\right] r \\ & + \frac{1}{15(1-v)}\left[(4-5v) r_{,k} n_m - (1-5v) r_{,m} n_k + [(4-5v)\delta_{mk} - r_{,m} r_{,k}]\frac{\partial r}{\partial n}\right] r^2\end{aligned} \tag{52}$$

The particular solution of the stress can be given as

$$\begin{aligned}\overline{\sigma}_{lkm} = {} & \frac{2(1-2v)}{5-4v}\left[\frac{1+v}{1-2v}\delta_{kl} r_{,m} + \frac{1}{2}(\delta_{mk} r_{,l} + \delta_{ml} r_{,k})\right] r \\ & + \frac{1}{15(1-v)}[(4-5v)(\delta_{mk} r_{,l} + \delta_{ml} r_{,k}) - (1-5v)\delta_{kl} r_{,m} - r_{,m} r_{,k} r_{,l}] r^2\end{aligned} \tag{53}$$

Solving Eqs. (46)–(48), the particular solution can be written as

$$u_i^p = \sum_{I=1}^{N+L} \begin{bmatrix} \overline{u}_{11}^I & \overline{u}_{12}^I \\ \overline{u}_{21}^I & \overline{u}_{22}^I \end{bmatrix} \begin{Bmatrix} \alpha_1^I \\ \alpha_2^I \end{Bmatrix} \tag{54}$$

$$t_i^p = \sum_{I=1}^{N+L} \begin{bmatrix} \overline{t}_{11}^I & \overline{t}_{12}^I \\ \overline{t}_{21}^I & \overline{t}_{22}^I \end{bmatrix} \begin{Bmatrix} \alpha_1^I \\ \alpha_2^I \end{Bmatrix} \tag{55}$$

Substituting Eq. (49) into Eqs. (54) and (55), one can obtain the particular solution in matrix form as

$$\mathbf{u^p} = \rho \mathbf{V} \mathbf{F}^{-1} \ddot{\mathbf{u}} \tag{56}$$

$$\mathbf{t^p} = \rho \mathbf{Q} \mathbf{F}^{-1} \ddot{\mathbf{u}} \tag{57}$$

where vector $\ddot{\mathbf{u}}$ is the value of acceleration on each node, $\mathbf{V}$ and $\mathbf{Q}$ are the matrices of the basic form of the particular solution.

4. Dual reciprocity hybrid boundary node method for elasto-dynamics

4.1. Basic equations

As the general solution and particular solution have been solved successfully for the differential equation of the dynamic problem, the general solution can be obtained.

In HBNM, MLS approximation is employed to construct the shape functions. Therefore, same as EFG method, there is an issue of imposition of the essential boundary condition as follows.

For edges, u_i and t_i are prescribed, respectively, as

$$\hat{u}_i = \sum_{J=1}^{N_t} R_{IJ} \tilde{u}_J = \sum_{J=1}^{N_t} R_{IJ} \overline{\overline{u}}_J \tag{58}$$

$$\hat{t}_i = \sum_{J=1}^{N_t} R_{IJ} \tilde{t}_J = \sum_{J=1}^{N_t} R_{IJ} \overline{\overline{t}}_J \tag{59}$$

where $R_{IJ} = [\Phi_J(s_I)]^{-1}$, N_t is the total number of the boundary nodes and $\overline{\overline{u}}_J$ and $\overline{\overline{t}}_J$ are the related nodal values.

Substituting Eq. (56) into Eq. (8), the general solution can be written as

$$\mathbf{u^c} = \mathbf{u} - \mathbf{u^p} = \mathbf{u} - \rho \mathbf{V} \mathbf{F}^{-1} \ddot{\mathbf{u}} \tag{60}$$

The corresponding expression for the traction $\mathbf{t^c}$ is

$$\mathbf{t^c} = \mathbf{t} - \mathbf{t^p} = \mathbf{t} - \rho \mathbf{Q} \mathbf{F}^{-1} \ddot{\mathbf{u}} \tag{61}$$

Substituting Eqs. (60) and (61) into Eqs. (58) and (59), and substituting the results further into Eqs. (41) and (42), one can obtain

$$\mathbf{T}\mathbf{x} = \mathbf{H}\mathbf{R}(\mathbf{t} - \mathbf{t^p}) = \mathbf{H}\mathbf{R}(\mathbf{t} - \rho \mathbf{Q} \mathbf{F}^{-1} \ddot{\mathbf{u}}) \tag{62}$$

$$\mathbf{U}\mathbf{x} = \mathbf{H}\mathbf{R}(\mathbf{u} - \mathbf{u^p}) = \mathbf{H}\mathbf{R}(\mathbf{u} - \rho \mathbf{V} \mathbf{F}^{-1} \ddot{\mathbf{u}}) \tag{63}$$

where matrix $\mathbf{R}$ is the transition matrix from Eqs. (58) and (59).

From Eq. (63), $\mathbf{x}$ can be expressed as

$$\mathbf{x} = \mathbf{U}^{-1} \mathbf{H}\mathbf{R}(\mathbf{u} - \rho \mathbf{V} \mathbf{F}^{-1} \ddot{\mathbf{u}}) \tag{64}$$

Substituting Eq. (64) into Eq. (62), one can obtain

$$\mathbf{T}\mathbf{U}^{-1} \mathbf{H}\mathbf{R}(\mathbf{u} - \rho \mathbf{V} \mathbf{F}^{-1} \ddot{\mathbf{u}}) = \mathbf{H}\mathbf{R}(\mathbf{t} - \rho \mathbf{Q} \mathbf{F}^{-1} \ddot{\mathbf{u}}) \tag{65}$$

Eq. (65) can be rewritten as

$$\mathbf{Ku} - \mathbf{Nt} + \mathbf{M\ddot{u}} = \mathbf{0} \tag{66}$$

where

$$\mathbf{K} = \mathbf{TU}^{-1}\mathbf{HR}$$

$$\mathbf{N} = \mathbf{HR}$$

$$\mathbf{M} = \rho(\mathbf{HRQF}^{-1} - \mathbf{TU}^{-1}\mathbf{HRVF}^{-1})$$

Eq. (66) is the system equation of DRHBNM for dynamics. It is initially partitioned according to the type of the applied boundary condition, and statically condensed in such a way that the final system could be solved for unknown displacements only.

According to Eq. (66), the system equation includes the acceleration which is related to the displacement in the domain. Denote the variables of the displacement and traction in boundary Γ_1 and Γ_2 as

$$\mathbf{u} = \begin{Bmatrix} \mathbf{u}_1 \\ \mathbf{u}_2 \\ \mathbf{u}_3 \end{Bmatrix}, \quad \mathbf{t} = \begin{Bmatrix} \mathbf{t}_1 \\ \mathbf{t}_2 \end{Bmatrix} \tag{67}$$

where $\mathbf{u_1}$ is the known and $\mathbf{t_1}$ is the unknown variables on Γ_1, $\mathbf{u_2}$ is the unknown and $\mathbf{t_2}$ is the known variables on Γ_2 and $\mathbf{u_3}$ is the unknown variable in the domain.

The global system, Eq. (66), can be partitioned as

$$\mathbf{K}_{11}\mathbf{u}_1 + \mathbf{K}_{12}\mathbf{u}_2 - \mathbf{N}_{11}\mathbf{t}_1 - \mathbf{N}_{12}\mathbf{t}_2 + \mathbf{M}_{11}\ddot{\mathbf{u}}_1 + \mathbf{M}_{12}\ddot{\mathbf{u}}_2 + \mathbf{M}_{13}\ddot{\mathbf{u}}_3 = \mathbf{0} \tag{68}$$

$$\mathbf{K}_{21}\mathbf{u}_1 + \mathbf{K}_{22}\mathbf{u}_2 - \mathbf{N}_{21}\mathbf{t}_1 - \mathbf{N}_{22}\mathbf{t}_2 + \mathbf{M}_{21}\ddot{\mathbf{u}}_1 + \mathbf{M}_{22}\ddot{\mathbf{u}}_2 + \mathbf{M}_{23}\ddot{\mathbf{u}}_3 = \mathbf{0} \tag{69}$$

From Eq. (68), the unknown traction $\mathbf{t_1}$ can be expressed in terms of other variables as

$$\mathbf{t}_1 = \mathbf{N}_{11}(\mathbf{K}_{11}\mathbf{u}_1 + \mathbf{K}_{12}\mathbf{u}_2 - \mathbf{N}_{12}\mathbf{t}_2 + \mathbf{M}_{11}\ddot{\mathbf{u}}_1 + \mathbf{M}_{12}\ddot{\mathbf{u}}_2 + \mathbf{M}_{13}\ddot{\mathbf{u}}_3) \tag{70}$$

Substituting the expression of $\mathbf{t_1}$ into Eq. (69), one finally obtains

$$\begin{aligned}(\mathbf{K}_{21} - \mathbf{N}_{21}\mathbf{N}_{11}^{-1}\mathbf{K}_{11})\mathbf{u}_1 + (\mathbf{K}_{22} - \mathbf{N}_{21}\mathbf{N}_{11}^{-1}\mathbf{K}_{12})\mathbf{u}_2 - (\mathbf{N}_{22} - \mathbf{N}_{21}\mathbf{N}_{11}^{-1}\mathbf{N}_{12})\mathbf{t}_2 \\ + (\mathbf{M}_{21} - \mathbf{N}_{21}\mathbf{N}_{11}^{-1}\mathbf{M}_{11})\ddot{\mathbf{u}}_1 + (\mathbf{M}_{22} - \mathbf{N}_{21}\mathbf{N}_{11}^{-1}\mathbf{M}_{12})\ddot{\mathbf{u}}_2 + (\mathbf{M}_{23} - \mathbf{N}_{21}\mathbf{N}_{11}^{-1}\mathbf{M}_{13})\ddot{\mathbf{u}}_3 = \mathbf{0}\end{aligned} \tag{71}$$

4.2. Free vibration analysis

For the free vibration analysis, the external loads and the displacement boundary conditions are set to be zero, i.e.,

$$\mathbf{u}_1 = \{\mathbf{0}\}, \quad \mathbf{t}_2 = \{\mathbf{0}\} \tag{72}$$

Substituting Eq. (72) into Eq. (71), the latter can be rewritten as

$$(\mathbf{K}_{22} - \mathbf{N}_{21}\mathbf{N}_{11}^{-1}\mathbf{K}_{12})\mathbf{u}_2 + (\mathbf{M}_{22} - \mathbf{N}_{21}\mathbf{N}_{11}^{-1}\mathbf{M}_{12})\ddot{\mathbf{u}}_2 + (\mathbf{M}_{23} - \mathbf{N}_{21}\mathbf{N}_{11}^{-1}\mathbf{M}_{13})\ddot{\mathbf{u}}_3 = \mathbf{0} \tag{73}$$

In Eq. (73), $\mathbf{u}_2$ are unknown on the boundary Γ_2 and $\ddot{\mathbf{u}}_3$ is unknown in the domain. Assuming the number of boundary unknown variables of $\mathbf{u}_2$ is N_k, from Eq. (73) one can get N_k equations. Also, L nodes are arranged in the domain, there have $2L$ unknown components. So the total number of the unknown variables $\mathbf{u}$ is $N_k + 2L$, and $2L$ additional equations should be compensated.

4.3. Additional equations

The displacement variables in the domain can be expressed as

$$\mathbf{u_3} = \mathbf{u^c} + \mathbf{u^p} = \hat{\mathbf{u}}\mathbf{x} + \rho\mathbf{V_I}\mathbf{F^{-1}}\ddot{\mathbf{u}} \tag{74}$$

where $\mathbf{u}_3$ are the displacements of the domain points, $\hat{\mathbf{u}}$ is the matrix that its components are the values of the fundamental solution on each domain point, $\mathbf{V_I}$ is the matrix that its components are the values of the basis form of the particular solution on each domain point.

The unknown coefficients of $\mathbf{x}$ in Eq. (74) can be solved by Eq. (64). Using Eq. (64), Eq. (74) can be rewritten as

$$\mathbf{u}_3 = \hat{\mathbf{u}}\mathbf{U}^{-1}\mathbf{HR}(\mathbf{u} - \rho\mathbf{VF}\ddot{\mathbf{u}}) + \rho\mathbf{V_I}\mathbf{F}^{-1}\ddot{\mathbf{u}} \tag{75}$$

where $\mathbf{u}$ is the displacement vector of the boundary points.

Eq. (75) can be rewritten as

$$\mathbf{Lu} - \mathbf{Iu}_3 + \mathbf{M_I}\ddot{\mathbf{u}} = \mathbf{0} \tag{76}$$

where $\mathbf{I}$ is a unit matrix, $\mathbf{L}$ and $\mathbf{M_I}$ are

$$\mathbf{L} = \hat{\mathbf{u}}\mathbf{U}^{-1}\mathbf{HR} \tag{77}$$

$$\mathbf{M_I} = \rho(\mathbf{V_I}\mathbf{F}^{-1} - \hat{\mathbf{u}}\mathbf{U}^{-1}\mathbf{HRVF}^{-1}) \tag{78}$$

As the same as Eqs. (68) and (69), Eq. (76) can be expressed by the known and unknown vectors of the displacements as

$$\mathbf{L}_1\mathbf{u}_1 + \mathbf{L}_2\mathbf{u}_2 - \mathbf{Iu}_3 + \mathbf{M}_{\mathbf{I}1}\ddot{\mathbf{u}}_1 + \mathbf{M}_{\mathbf{I}2}\ddot{\mathbf{u}}_2 + \mathbf{M}_{\mathbf{I}3}\ddot{\mathbf{u}}_3 = \mathbf{0} \tag{79}$$

As $\mathbf{u_1}$ equals to zero, Eq. (79) can be rewritten as

$$\mathbf{L}_2\mathbf{u}_2 - \mathbf{Iu}_3 + \mathbf{M}_{\mathbf{I}2}\ddot{\mathbf{u}}_2 + \mathbf{M}_{\mathbf{I}3}\ddot{\mathbf{u}}_3 = \mathbf{0} \tag{80}$$

These are the additional equations for the solution.

4.4. Final system equations

Combining Eqs. (73) and (80), one can obtain

$$\hat{\mathbf{H}}\mathbf{u_4} + \hat{\mathbf{M}}\ddot{\mathbf{u}}_4 = \mathbf{0} \tag{81}$$

where $\mathbf{u_4}$ is a vector that combines $\mathbf{u_2}$ and $\mathbf{u_3}$, matrices $\hat{\mathbf{H}}$ and $\hat{\mathbf{M}}$ can be written as

$$\hat{\mathbf{H}} = \begin{bmatrix} \mathbf{K}_{22} - \mathbf{N}_{21}\mathbf{N}_{11}^{-1}\mathbf{K}_{12} & \mathbf{0} \\ \mathbf{L}_2 & -\mathbf{I} \end{bmatrix} \tag{82}$$

$$\hat{\mathbf{M}} = \begin{bmatrix} \mathbf{M}_{22} - \mathbf{N}_{21}\mathbf{N}_{11}^{-1}\mathbf{M}_{12} & \mathbf{M_{23}} - \mathbf{N}_{21}\mathbf{N}_{11}^{-1}\mathbf{M}_{13} \\ \mathbf{M}_{\mathbf{I}2} & \mathbf{M}_{\mathbf{I}3} \end{bmatrix} \tag{83}$$

Assuming the displacement $\mathbf{u_4}$ is the harmonic function of time, thus

$$\ddot{\mathbf{u}}_4 = -\omega^2\mathbf{u}_4 \tag{84}$$

with ω being the natural circular frequency. Eq. (81) is then reduced to

$$\hat{\mathbf{H}}\mathbf{u_4} = \omega^2\hat{\mathbf{M}}\mathbf{u_4} \tag{85}$$

which represents the generalized algebraic eigenvalue problem. It should be pointed out that neither $\hat{\mathbf{H}}$ nor $\hat{\mathbf{M}}$ are symmetric or positive definite, so that care should be taken in the choice of the appropriate eigenvalue solution algorithm.

The method employed by Nardini and Brebbia [29] reduced the generalized eigenvalue problem to a standard one by the inversion of matrix $\hat{\mathbf{H}}$, and obtained the following system:

$$\mathbf{Au}_4 = \lambda\mathbf{u}_4 \tag{86}$$

with

$$\mathbf{A} = \hat{\mathbf{H}}^{-1}\hat{\mathbf{M}} \tag{87}$$

$$\lambda = \frac{1}{\omega^2} \tag{88}$$

From the above development, one can see that the present method is a true meshless one, as absolutely no boundary elements are needed, either for interpolation purpose or for integration purpose. The nodes in the domain are necessary just for interpolation of the particular solution and are not needed for the domain integral.

5. Numerical implementation

5.1. Singular integral

It is obvious that the integrals in Eqs. (43) and (45) consist of regular and singular ones. The regular integrals can be evaluated using the usual Gaussian quadrature based on the regular boundary Γ_s. The singular integrals in Eqs. (43) and (45) are different and they should be treated by different methods.

The main diagonal term of matrix $\mathbf{U}$ in Eq. (45) involves a logarithm singular integral. This type of singular integral can be calculated by a modified Gauss quadrature as follows:

$$I = \int_0^1 \ln\left(\frac{1}{\xi}\right) f(\xi)\,\mathrm{d}\xi = \sum_{i=1}^{n} f(\xi_i) w_i \tag{89}$$

where ξ_i and w_i are the integration points and weight factors, respectively. They are the same as the conventional BEM.

However, the main diagonal terms of matrix $\mathbf{T}$ in Eq. (43) involves a $(1/r)$ type singular integral and cannot be dealt with by the usual method directly. In order to avoid the calculation of hyper-singular integral, the rigid body moving method is applied as BEM.

For a plane strain problem, two groups of particular solutions of rigid body force are applied. They are both constant displacement fields and can be described as follows:

$$u_1 = 0, \quad u_2 = 1, \quad t_1 = t_2 = 0 \tag{90}$$

$$u_1 = 1, \quad u_2 = 0, \quad t_1 = t_2 = 0 \tag{91}$$

where 1 and 2 represent the direction of x and y, respectively.

Substituting Eqs. (90) and (91) into Eqs. (41) and (42), one can obtain

$$\mathbf{T}\mathbf{U}^{-1}\mathbf{H}\{\mathbf{u}\} = \mathbf{H}\{\mathbf{0}\} \tag{92}$$

where $\{\mathbf{0}\}$ is a column vector with all elements equal to zero. Substituting the two groups of the displacement particular solutions into Eq. (92), respectively, the values of the main diagonal of $\mathbf{T}$ can be obtained.

5.2. Eigenvalue and eigenvector

From the above analysis, one can see that matrix $\mathbf{A}$ is nonsymmetrical. The Q-R algorithm is chosen to solve all natural circular frequencies. In order to improve the convergence, matrix $\mathbf{A}$ is transformed firstly into tri-diagonal form by the Householder algorithm. Then the eigenvalues and eigenvectors of the transformed matrix are calculated by the Q–R algorithm. For the large systems, a variant of the sub-space iteration method is used for the nonsymmetric matrices [22,23].

The Q–R algorithm is described as following.

Assume $\mathbf{A_1} = \mathbf{A}$, note $\mathbf{A_r} = [a_{ij}^{(r)}]_{n\times n}$, and set $\mathbf{Q_1} = \mathbf{I}$, where $\mathbf{I}$ is a unit matrix. For $r = 1, 2, 3, \ldots, n-1$, calculate the following equations:

(1) If $a_{ir}^{(r)} (r = r+1, r+2, \ldots, n)$ are equal to zero, assume $\mathbf{Q_{r+1}} = \mathbf{Q_r}$, $\mathbf{A_{r+1}} = \mathbf{A_r}$, and go to (5), otherwise go to (2).

(2) Calculate the following equations:

$$d_r = \sqrt{\sum_{i=r}^{n} (a_{ir}^{(r)})^2}$$

$$c_r = -\mathrm{sign}(a_{rr}^{(r)}) d_r$$

If $a_{rr}^{(r)} = 0$, then note $c_r = d_r$

$$h_r = c_r^2 - c_r a_{rr}^{(r)}$$

(3) Assume $\mathbf{u_r} = (0, \ldots, 0, a_{rr}^{(r)} - c_r, a_{r+1,r}^{(r)}, \ldots, a_{n,r}^{(r)})^{\mathrm{T}}$

(4) Calculate $\omega_{\mathbf{r}} = \mathbf{Q_r u_r}$

$$\mathbf{Q_{r+1}} = \mathbf{Q_r} - \omega_{\mathbf{r}} \mathbf{u_r^T} / h_r$$

$$\mathbf{P_r} = \mathbf{A_r^T u_r} / h_r$$

$$\mathbf{A_{r+1}} = \mathbf{A_r} - \mathbf{u_r P_r^T}$$

(5) If $r = n-1$, stop calculation, otherwise go to (1).

If calculation is over, an upper triangular matrix $\mathbf{A}$ is obtained, and $\mathbf{A} = \mathbf{QR}$, the eigenvalue of $\mathbf{A}$ is the same as the original matrix. Based on the above, an iteration method is obtained as

$$\begin{cases} \mathbf{A}_1 = \mathbf{A} \\ \mathbf{A_k} = \mathbf{Q_k R_k} \qquad \text{(Decomposition } \mathbf{A_K} \text{ by the Q}-\text{R algorithm)} \\ \mathbf{A_k} = \mathbf{A_{k+1} Q_k} \end{cases}$$

If iteration is over, the elements under the diagonal are close to zero, and the diagonal elements are eigenvalues.

6. Numerical examples

A number of examples are presented to illustrate the effectiveness of this method for free vibration analysis. The parameters that influence the performance of the method are also investigated. The results of the present method are compared with both the analytical solutions and those of FEM software ANSYS.

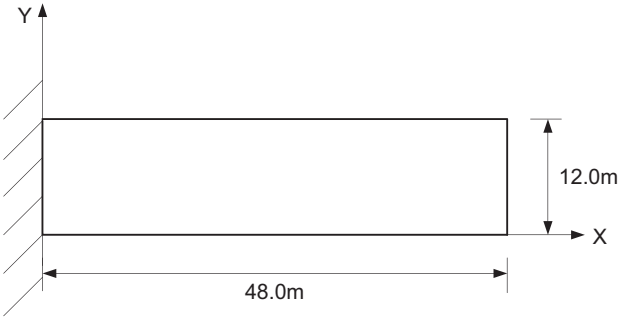

Fig. 2. A cantilever.

In these examples, the support size for the weight function d_I is taken to be $3.5h$ and the radius of the sub-domain r_J is chosen as $0.85h$, with h being the average distance of the adjacent nodes. The parameter c_I is taken to be $d_I/c_I = 0.5$, and the parameter c_J is taken to be $r_I/c_J = 1.2$. To deal with the traction discontinuities at the corners, the nodes are not arranged at these locations and the support domain for interpolation is truncated.

6.1. A cantilever

Consider the free vibration of a cantilever shown in Fig. 2. The left side is clamped and plane stress condition is assumed. The length of the cantilever is 48.0 m, the height is 12.0 m and the thickness is 1.0 m.

Table 1
First five natural circular frequencies of the cantilever.

Mode	Present method (Hz)	EFG [28] (Hz)	FEM (ANSYS; Hz)
1	27.71	27.72	27.71
2	140.84	140.83	140.86
3	179.70	179.71	179.71
4	323.75	323.71	323.88
5	523.46	522.90	523.43

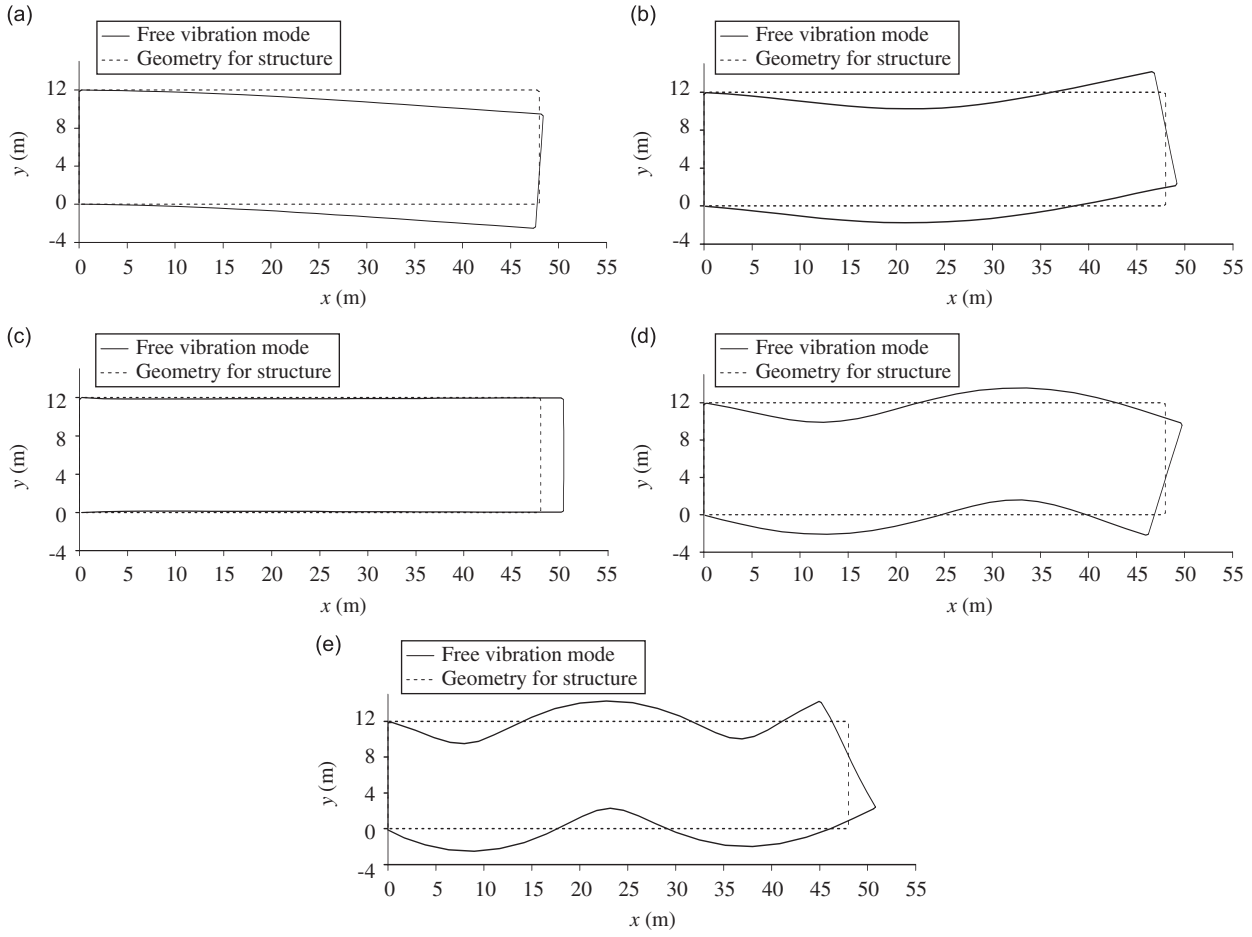

Fig. 3. First five free vibration modes of the cantilever: (a) first free vibration mode; (b) second free vibration mode; (c) three free vibration mode; (d) forth free vibration mode; (e) fifth free vibration mode.

The material constants are given as $\rho = 2000\,\mathrm{kg/m^3}$, $E = 6.0 \times 10^{10}\,\mathrm{Pa}$ and $v = 0.3$. The cantilever is discretized using 24 nodes on each long edge and eight nodes on each short edge. A total of 64 boundary nodes are located on the boundary and 24 internal nodes are arranged in the domain.

The natural circular frequencies for the first five natural modes are given in Table 1. In order to check the effectiveness of the method, the present results are compared with those of FEM and EFG [28]. In FEM analysis by ANSYS, 4608 elements were used, and in EFG analysis, 189 nodes were used. It can be seen that even though the number of nodes is relatively small, a good result still can be obtained by the present method.

According to the first five natural circular frequencies, the corresponding free vibration modes have been calculated and shown in Fig. 3.

6.2. Arch with both ends built-in

The arch with both ends built-in is depicted in Fig. 4. This is assumed as a plane stress problem and the thickness is 0.1 m. The dimensions and material constants are given as $r_0 = 2.5\,\mathrm{m}$, $r_1 = 5.0\,\mathrm{m}$, $E = 2 \times 10^7\,\mathrm{Pa}$, $\rho = 2000\,\mathrm{kg/m^3}$ and $v = 0.25$. Twenty nodes are arranged on the external arch boundary and 10 nodes are on the inner arch boundary, five nodes are located on each fixed edge. A total 40 nodes are arranged on the boundary and 30 internal nodes are used for interpolation.

The first five natural circular frequencies are given in Table 2. For comparison, BEM and FEM are applied to calculate this structure at the same time. Twenty-two boundary elements are used in BEM and 400 and 200 elements are used, respectively, in two cases of FEM calculation. Again, a good agreement of the natural frequencies obtained by the present method, BEM [29] and FEM can be achieved.

According to the first five natural circular frequencies, the corresponding free vibration modes calculated by the present method are shown in Fig. 5. Those obtained by FEM are shown in Fig. 6. It can be seen that the results for each mode obtained by the two methods agree generally. It is shown that although the present method used much less nodes that FEM, it can still obtain more accurate results.

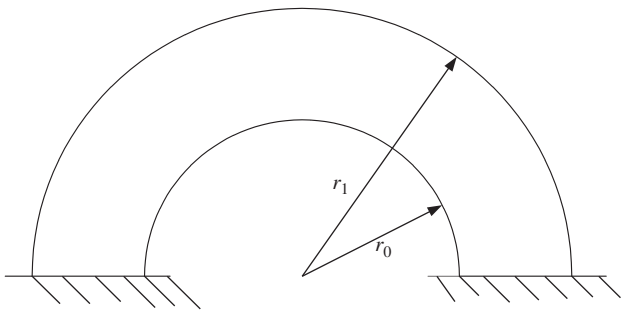

Fig. 4. An arch.

Table 2
First five natural circular frequencies of the arch.

Mode	Present method (Hz)	BEM [29] (Hz)	FEM (ANSYS; 400 elements; Hz)	FEM (ANSYS; 200 elements; Hz)
1	14.401	14.580	14.415	14.200
2	21.713	21.420	21.734	21.132
3	33.657	33.580	33.690	32.818
4	36.724	37.780	36.730	36.103
5	51.389	51.010	51.395	51.119

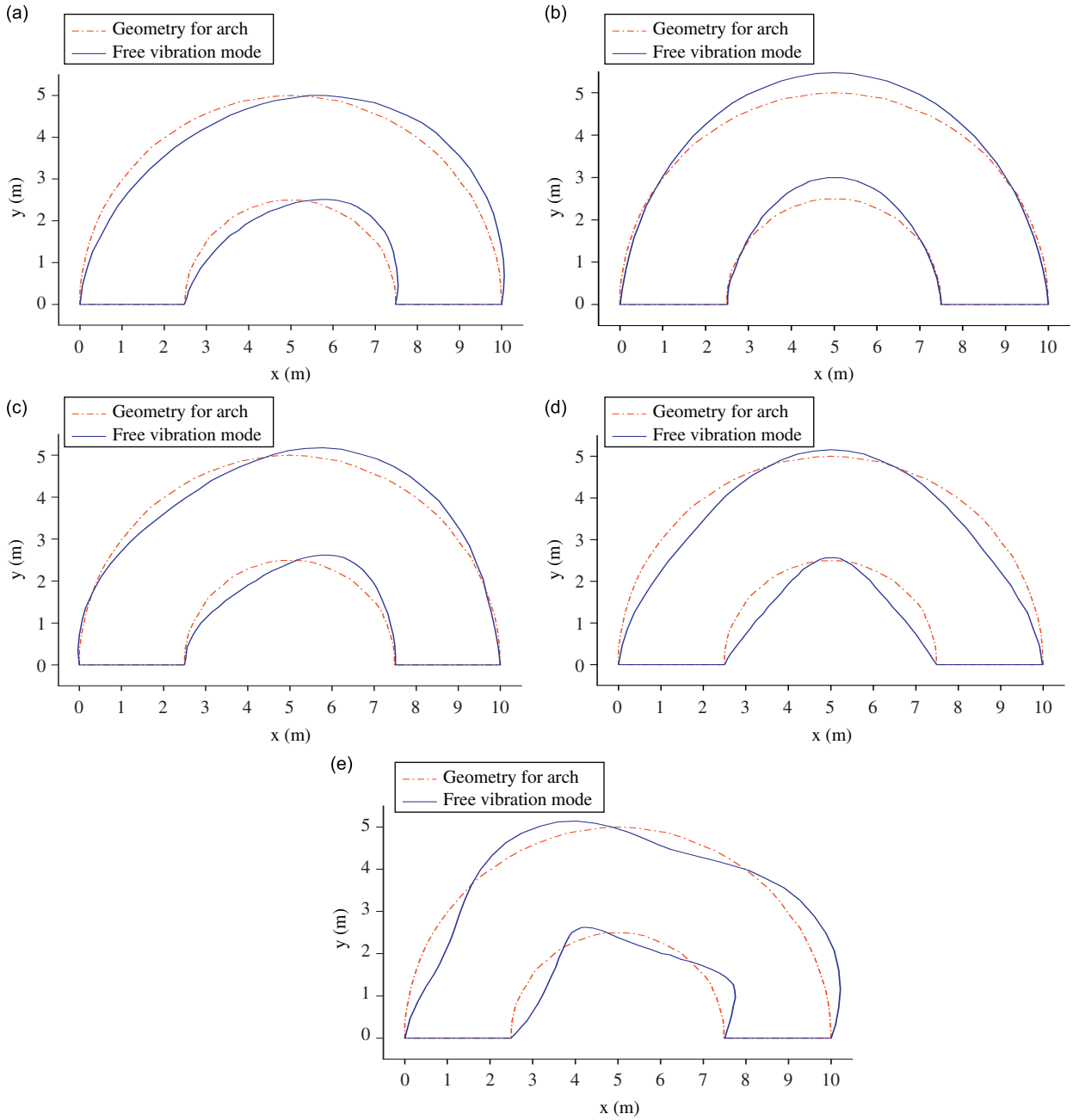

Fig. 5. First five free vibration modes of the arch by the present method: (a) first free vibration mode; (b) second free vibration mode; (c) three free vibration mode; (d) forth free vibration mode; (e) fifth free vibration mode.

6.3. A roadbed

A roadbed with a trapeze cross section is shown in Fig. 7. The base width is 12 m and the height and the top width are 4 m. This is assumed as a plane strain problem and the material constants are $\rho = 2400\,\mathrm{kg/m^3}$, $E = 4 \times 10^8\,\mathrm{Pa}$ and $v = 0.3$. Six nodes are arranged on the top, 18 nodes are on the bottom and eight nodes are on the left and right slopes of the roadbed, respectively. Total 40 nodes are located on the boundary and 21 internal nodes are arranged in the domain.

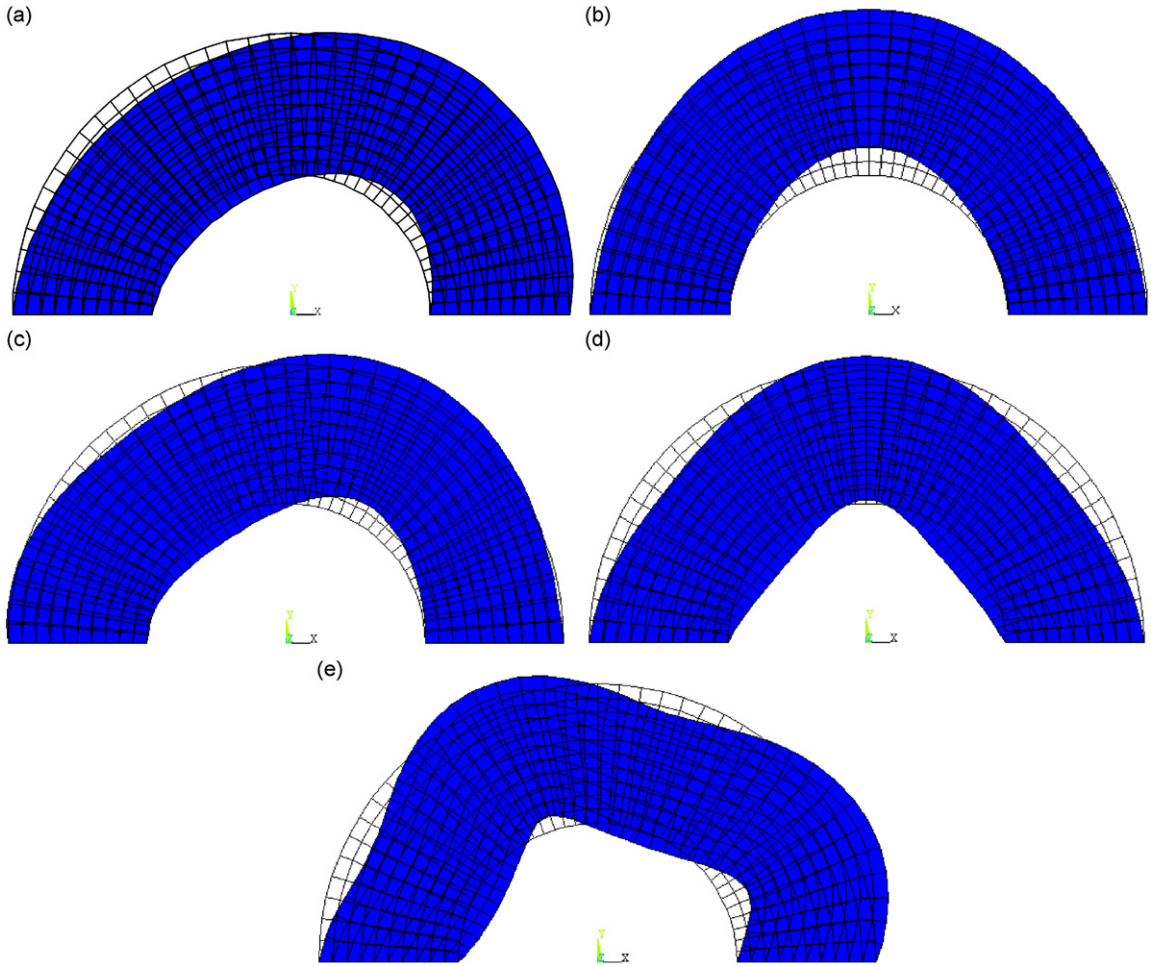

Fig. 6. First five free vibration modes of the arch by ANSYS: (a) first free vibration mode; (b) second free vibration mode; (c) three free vibration mode; (d) forth free vibration mode; (e) fifth free vibration mode.

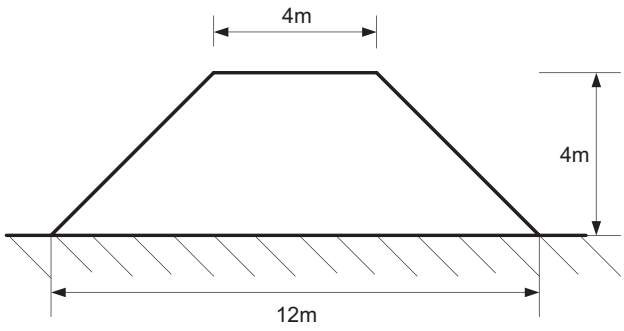

Fig. 7. A roadbed.

The first five natural circular frequencies are listed in Table 3. For comparison, FEM is applied to calculating this structure and 1500 elements are used. Again, good agreement of the natural frequencies for each mode obtained by the present method and ANSYS can be noted, with a small number of nodes in the

Table 3
First five natural circular frequencies of the roadbed.

Mode	Present method (Hz)	FEM (ANSYS; Hz)
1	114.8156	114.7624
2	186.8657	186.3467
3	212.2789	212.4848
4	248.4817	248.8481
5	270.3037	269.8251

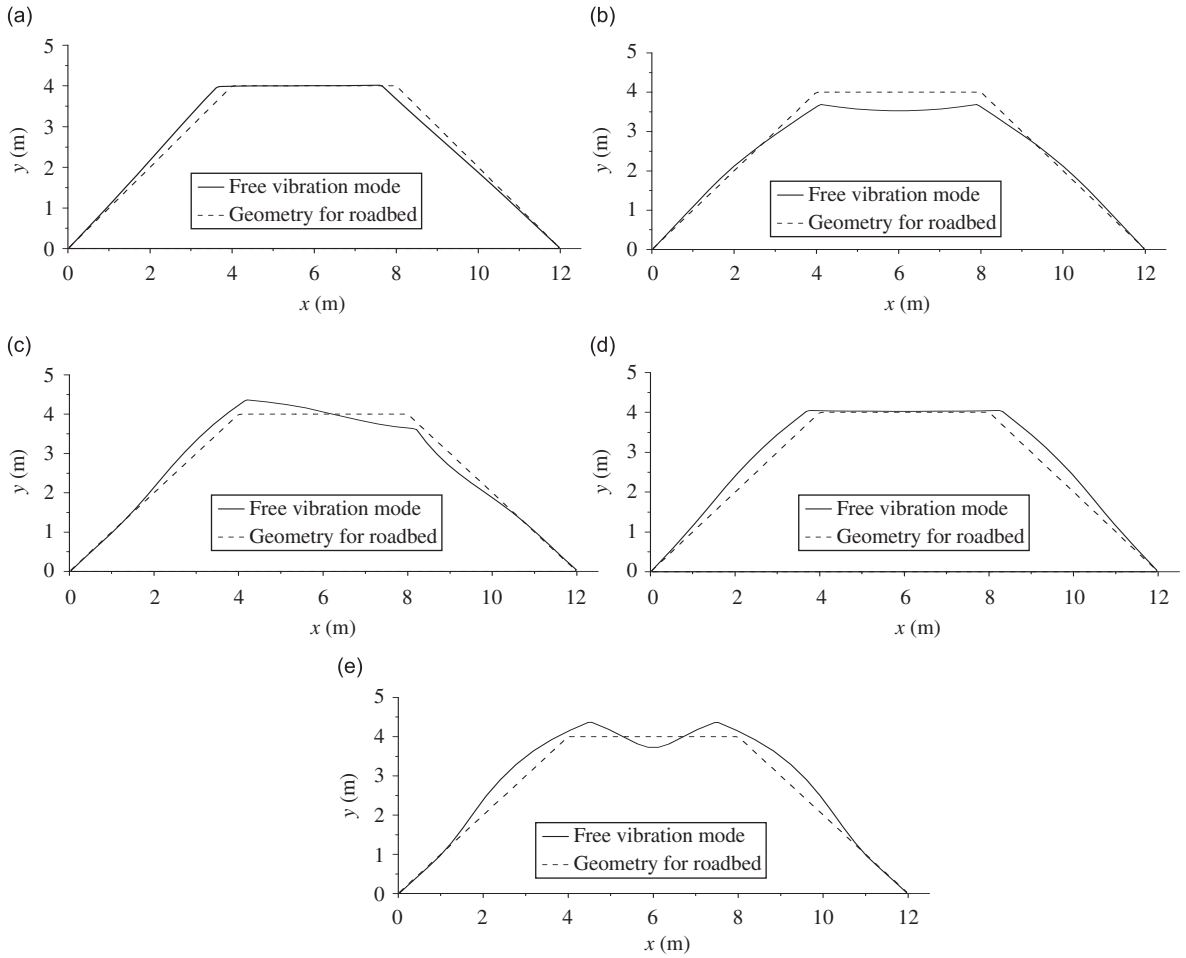

Fig. 8. First five free vibration modes of the roadbed: (a) first free vibration mode; (b) second free vibration mode; (c) three free vibration mode; (d) forth free vibration mode; (e) fifth free vibration mode.

present method. A total of 61 nodes are used in the present method and 1500 elements are used in ANSYS. It is obvious that the computation amount for precondition of the present method is much less than that of ANSYS, and the results are more accurate and efficient.

According to the first five natural circular frequencies, the corresponding free vibration modes are calculated and shown in Fig. 8.

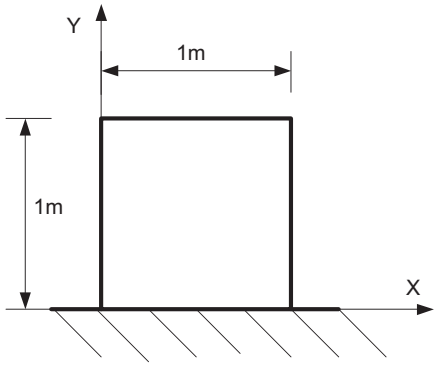

Fig. 9. Cross section of the dam.

Table 4
First two natural circular frequencies of the dam.

Mode	Present method (Hz)	FEM (ANSYS; Hz)
1	690.50	691.00
2	1571.51	1571.00

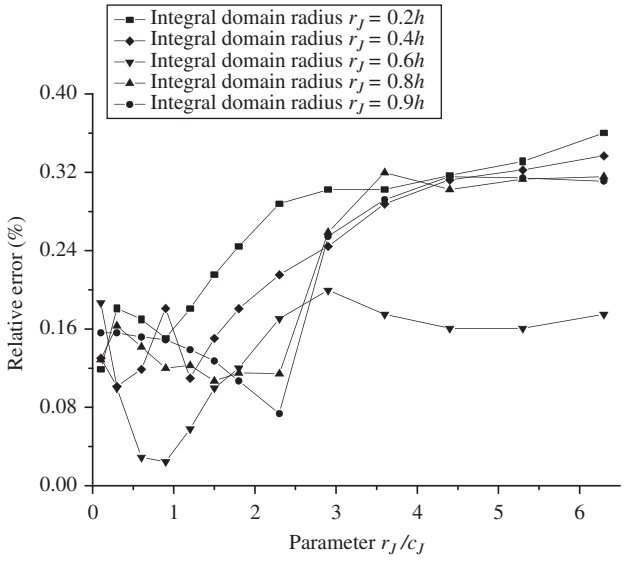

Fig. 10. Relative error of the first natural circular frequency for different r_J.

6.4. Parameter study

The influence of the computation parameters will be studied in this section. As shown in Fig. 9, a dam with a square section is taken as the example. This is assumed as a plane strain problem and the side length of the side is 1.0 m, and the base is fixed. The material parameters are $\rho = 2000\,\mathrm{kg/m^3}$, $E = 2.0 \times 10^9\,\mathrm{Pa}$ and $\nu = 0$.

In order to check the effectiveness of the method, the results of the first two frequencies obtained by the present method and FEM are given in Table 4. In the present calculation, the dam is discretized using 15 nodes

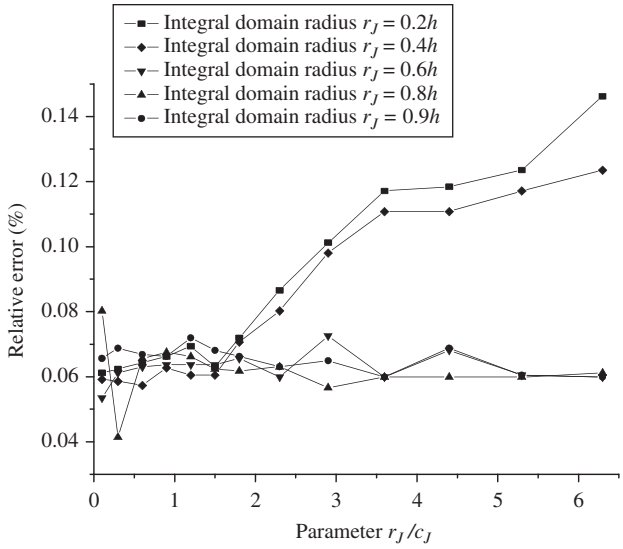

Fig. 11. Relative error of the second natural circular frequency for different r_J.

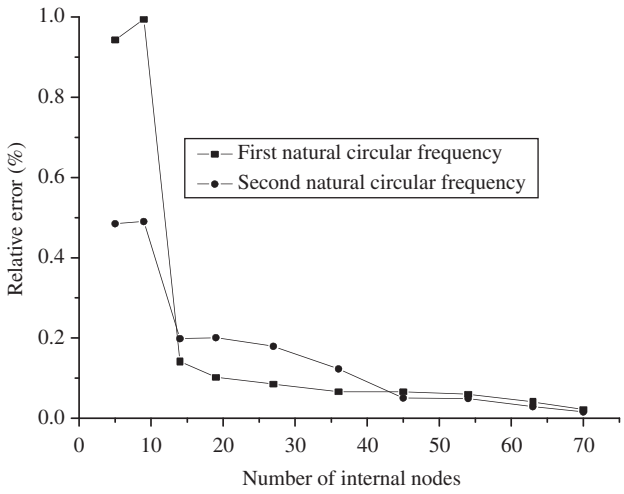

Fig. 12. Relative error of the natural frequency for different internal nodes.

on each side and a total of 36 internal nodes are arranged in the domain. The calculation parameters are $r_J = 0.8h$ and $r_J/c_J = 1.2$. In FEM analysis, there are 2500 elements used by ANSYS software. It can be seen that although the node number of the present method is much less than that for ANSYS analysis, the agreement of the two methods is still excellent.

For different parameter r_J, the relative error of the first and second natural circular frequencies are shown in Figs. 10 and 11. The relative error of the first natural circular frequency is less than 0.35%, and the relative error of the second natural circular frequency is less than 0.15%. It can be seen that the influence of the parameter is not significant. When $r_J \geqslant 0.5h$ and $0.1 \leqslant r_J/c_J \leqslant 1.5$, the computation error is rather small.

The influence of the internal nodes is present in Fig. 12. It can be seen that the more the points are arranged in the domain, the more the accurate solution can be obtained. It shows that when more than 15 internal nodes are used, the relative error is always very small.

7. Conclusions

A new boundary-type meshless method, DRHBNM, has been proposed for the dynamic analysis of structures. It combines HBNM and DRM, where HBNM is used to obtain the general solution without inhomogeneous terms and DRM is employed to deal with the inhomogeneous terms and obtain the particular solution. Detailed formulations for solving free vibration problems are developed. The boundary integral equation is discretized using the meshless shape functions based on a group of arbitrarily distributed points on the boundary. The points in the domain are only used to interpolate particular solution by the radial basis function, and not necessary for integration and approximation of the variables. Some additional equations are proposed to get the connection between the boundary variables and internal variables.

A series of examples have been given. The numerical results have demonstrated the accuracy, convergence and effectiveness of the present method. This method is used to calculate the natural circular frequencies and free vibration modes of different structures, and can be applied for the damping vibration and dynamic response analysis. It can be applied further for the 3-D dynamic problems.

Compared to the element methods such as FEM and BEM, DRHBNM is a truly meshless method. It does not need elements meshing and is suitable for the dynamic crack problems. Besides, accuracy and convergence are very high. The numerical examples show that although much less amount of nodes are used, very good results can be obtained comparing with FEM. For free vibration problems, only some nodes are needed for the analysis, the meshing work is much less, especial for some complex geometry structures. This means that the precondition and post treatment are easier than that of FEM.

The influences of the computer parameters, such as the size of the sub-domain radius and the number of the internal nodes are studied. The optimal value of the radius of the sub-domain is greater than $0.5h$. The influence of the parameter r_J/c_J is insignificant and can be chosen from 0.1 to 1.5. Also, the internal points are only used for the interpolation of the particular function. The suitable number of the internal nodes can satisfy the calculation accuracy. The results show that the method has good wide suitability.

Acknowledgments

The financial support from The University of Hong Kong is greatly appreciated. This work was supported by Natural Science Foundation of China (no. 50808090).

References

[1] O.C. Zienkiewicz, *Finite Element Method*, McGraw-Hill, London, 1977.
[2] C.A. Brebbia, J. Dominguez, *Boundary Elements—An Introductory Course*, second ed., McGraw-Hill, New York, 1992.
[3] B. Nayroles, G. Touzot, P. Villon, Generalizing the finite element method: diffuse approximation and diffuse element, *Computational Mechanics* 10 (1992) 307–318.
[4] T. Belytschko, Y.Y. Lu, L. Gu, Element-free Galerkin methods, *International Journal for Numerical Methods in Engineering* 137 (1994) 229–256.
[5] W.K. Liu, Y. Chen, R.A. Uras, C.T. Chang, Generalized multiple scale reproducing kernel particle methods, *Computer Methods in Applied Mechanics and Engineering* 139 (1996) 91–157.
[6] G.R. Liu, Y.T. Gu, A local point interpolation method for stress analysis of two-dimensional solids, *Structural Engineering and Mechanics* 11 (2001) 221–236.
[7] S.N. Atluri, T. Zhu, A new meshless local Petrov–Galerkin approach in computational mechanics, *Computational Mechanics* 22 (1998) 117–127.
[8] Y.T. Gu, G.R. Liu, A coupled element free Galerkin/boundary element method for stress analysis of two-dimensional solids, *Computer Methods in Applied Mechanics and Engineering* 190 (2001) 4405–4419.
[9] S. De, K.J. Bathe, The method of finite spheres with improved numerical integration, *Computers & Structures* 79 (2001) 2183–2196.
[10] N.R. Aluru, G. Li, Finite cloud method: a true meshless technique based on a fixed reproducing kernel approximation, *International Journal for Numerical Methods in Engineering* 50 (2001) 2373–2410.
[11] T. Zhu, A new meshless regular local boundary integral boundary integral equation approach, *International Journal for Numerical Methods in Engineering* 146 (1999) 1237–1252.
[12] Y.X. Mukherjee, S. Mukherjee, The boundary node method for potential problems, *International Journal for Numerical Methods in Engineering* 140 (1994) 797–815.

[13] W. Cheri, M. Tanaka, A meshless, integration-free, boundary-only RBF technique, *Computers & Mathematics with Applications* 43 (2002) 379–391.
[14] G.R. Liu, *Mesh-Free Methods: Moving Beyond the Finite Element Method*, CRC Press, Boca Raton, FL, 2002.
[15] Y.X. Mukherjee, S. Mukherjee, The boundary node method for potential problems, *International Journal for Numerical Methods in Engineering* 40 (1997) 797–815.
[16] J.M. Zhang, Z.H. Yao, H. Li, A hybrid boundary node method, *International Journal for Numerical Methods in Engineering* 53 (2002) 751–763.
[17] J.M. Zhang, Z.H. Yao, T. Masataka, The meshless regular hybrid boundary node method for 2-D linear elasticity, *Engineering Analysis with Boundary Elements* 127 (2003) 259–268.
[18] H.T. Wang, Z.H. Yao, S. Cen, A meshless singular hybrid boundary node method for 2-D elastostatics, *Journal of the Chinese Institute of Engineers* 27 (2004) 481–490.
[19] J.M. Zhang, T. Masataka, M. Toshiro, Meshless analysis of potential problems in three dimensions with the hybrid boundary node method, *International Journal for Numerical Methods in Engineering* 59 (2004) 1147–1168.
[20] J.M. Zhang, Z.H. Yao, The regular hybrid boundary node method for three-dimensional linear elasticity, *Engineering Analysis with Boundary Elements* 28 (2004) 525–534.
[21] J.M. Zhang, Z.H. Yao, Meshless regular hybrid boundary node method, *Computer Modeling in Engineering & Sciences* 2 (2001) 307–318.
[22] Y. Miao, Y.H. Wang, F. Yu, Development of hybrid boundary node method in two-dimensional elasticity, *Engineering Analysis with Boundary Elements* 29 (2005) 703–712.
[23] D. Nardini, C.A. Brebbia, A New Approach to Free Vibration Analysis using Boundary Elements, *Boundary Element Methods in Engineering*, Computational Mechanics Publications, Southampton, Springer, Berlin, New York, 1982.
[24] L.C. Wrobel, C.A. Brebbia, The dual reciprocity boundary element formulation for non-linear diffusion problems, *Computer Methods in Applied Mechanics and Engineering* 65 (1987) 147–164.
[25] D. Nardini, C.A. Brebbia, Boundary integral formulation of mass matrices for dynamic analysis, *Topics in Boundary Element Research*, Vol. 2, Springer, Berlin, New York, 1985.
[26] D. Nardini, C.A. Brebbia, Transient boundary element elastodynamics using the dual reciprocity method and modal superposition, *Boundary Elements*, Vol. 1, Computational Mechanics Publications, Southampton, Springer, Berlin, New York, 1986.
[27] S.B. Dong, A Block-Stodola eigensolution technique for large algebraic systems with non-symmetrical matrices, *International Journal for Numerical Methods in Engineering* 11 (1977) 247–269.
[28] C.B. Ren, G.Z. He, A meshless precise integration method to solve a 2-D structural vibration problem, *Journal of Vibration and Shock* 26 (2007) 126–129.
[29] P.W. Partridge, C.A. Brebbia, L.C. Wrobel, *The Dual Reciprocity Boundary Element Method*, Computational Mechanics Publications, Southampton, Boston Co-published with Elsevier Applied Science, London, New York, 1992.